Supporting Information for

Distinct stadial-interstadial amplitudes of Asian monsoon water isotopes during the last deglaciation

Xiaoqing Wang[1,2], Weiyi Sun[1,2*], Jian Liu[1,2], Liang Ning[1,2], Yuntao Bao[3,4], Kan Zhao[1,2], Jiazhi He[1,2], Yanan Ma[1,2], Kefan Chen[1,2], Qin Wen[1,2], and Yongjin Wang[1,2]

[1] State Key Laboratory of Climate System Prediction and Risk Management, Key Laboratory for Virtual Geographic Environment of Ministry of Education, Jiangsu Center for Collaborative Innovation in Geographical Information Resource Development and Application, Nanjing Normal University, Nanjing, China

[2] School of Geography, Nanjing Normal University, Nanjing, China

[3] Nanjing-Helsinki Institute in Atmospheric and Earth System Sciences, Nanjing University, Nanjing, China

[4] Department of Geography, The Ohio State University, Columbus, Ohio, USA

*Corresponding authors: Weiyi Sun, weiyisun@njnu.edu.cn

Contents of this file:

Supplementary Table 1 Summary of compiled speleothem $\delta^{18}O$ records

Site	Lat (°N)	Lon (°E)	Reference
Southeastern Yunnan caves	23.50	104.00	1
Coastal Bay of Bengal caves	15.92	99.45	1
Mawmluh Cave	25.26	91.82	2
Xiaobailong Cave	24.20	103.35	3
Furong Cave	29.23	107.90	4
Luoshui Cave	29.73	110.17	5
Hulu Cave	32.50	119.16	6, 7
Haozhu Cave	30.68	109.98	8

Supplementary Table 2 Summary of compiled multi-proxy precipitation records

Site	Proxy	Lat (°N)	Lon (°E)	Reference
Northeastern Arabian Sea	Reflectance	23.12	66.5	9
Tengchongqinghai Lake	Pollen	25.12	98.57	10
Caohai Lake	Pollen	26.81	104.34	10
Gulang	Loess	37.49	102.88	11
Jingyuan	Loess	36.35	104.62	11
Gonghai Lake	Pollen	38.90	112.23	12
Haozhu Cave	Speleothems	30.68	109.98	8
Gutian	Pollen	26.08	110.37	13

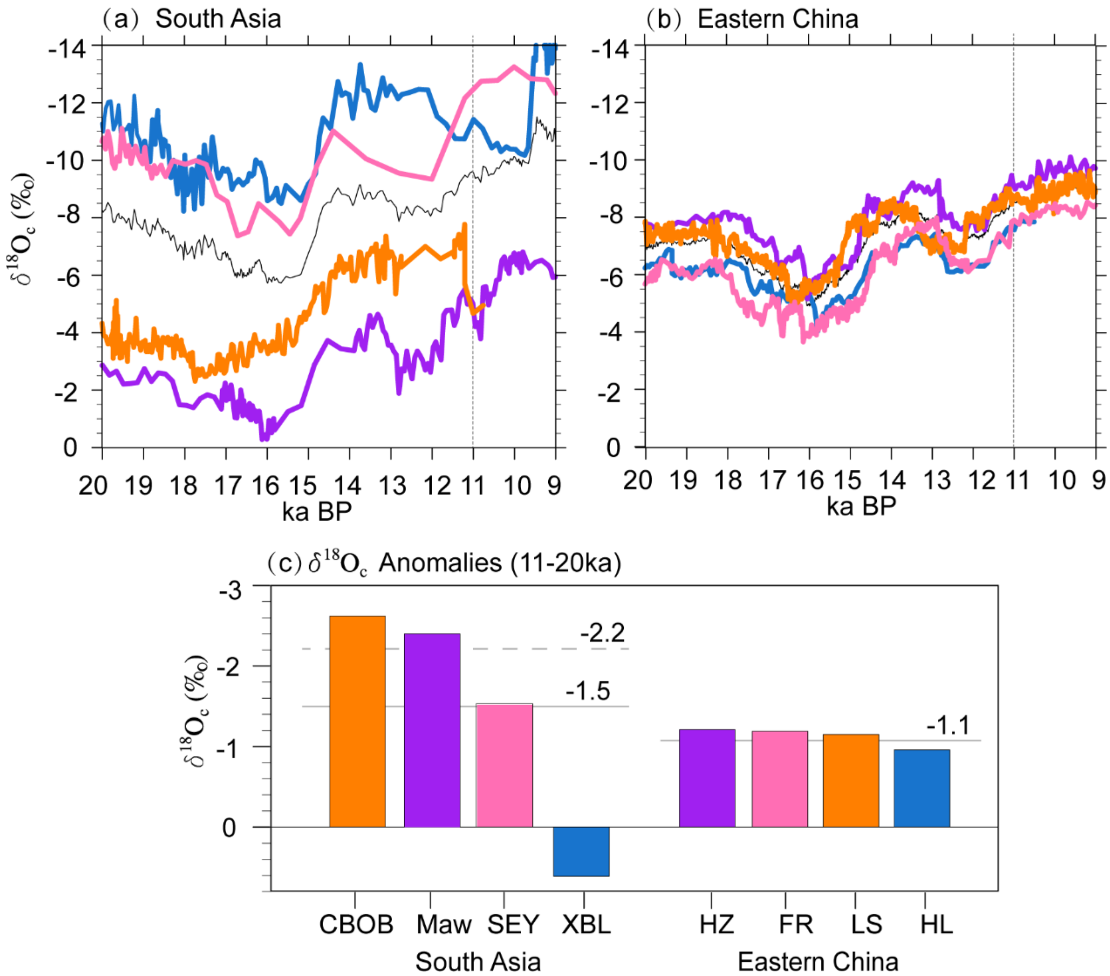

Supplementary Fig. 1 | Speleothem $\delta^{18}O_c$ records from South Asia and East China. Time series of speleothem $\delta^{18}O_c$ records in (**a**) South Asia and (**b**) East China during 20 to 9 ka. Line colors correspond to the records shown in Fig. 1b–c. The grey vertical dashed line marks the time of 11 ka. (**c**) Bar heights show the $\delta^{18}O_c$ anomalies for each record during 20 to 11 ka, with colors matching the time series. The gray solid and dashed lines denote the mean anomalies for all records and excluding the XBL record[3], respectively.

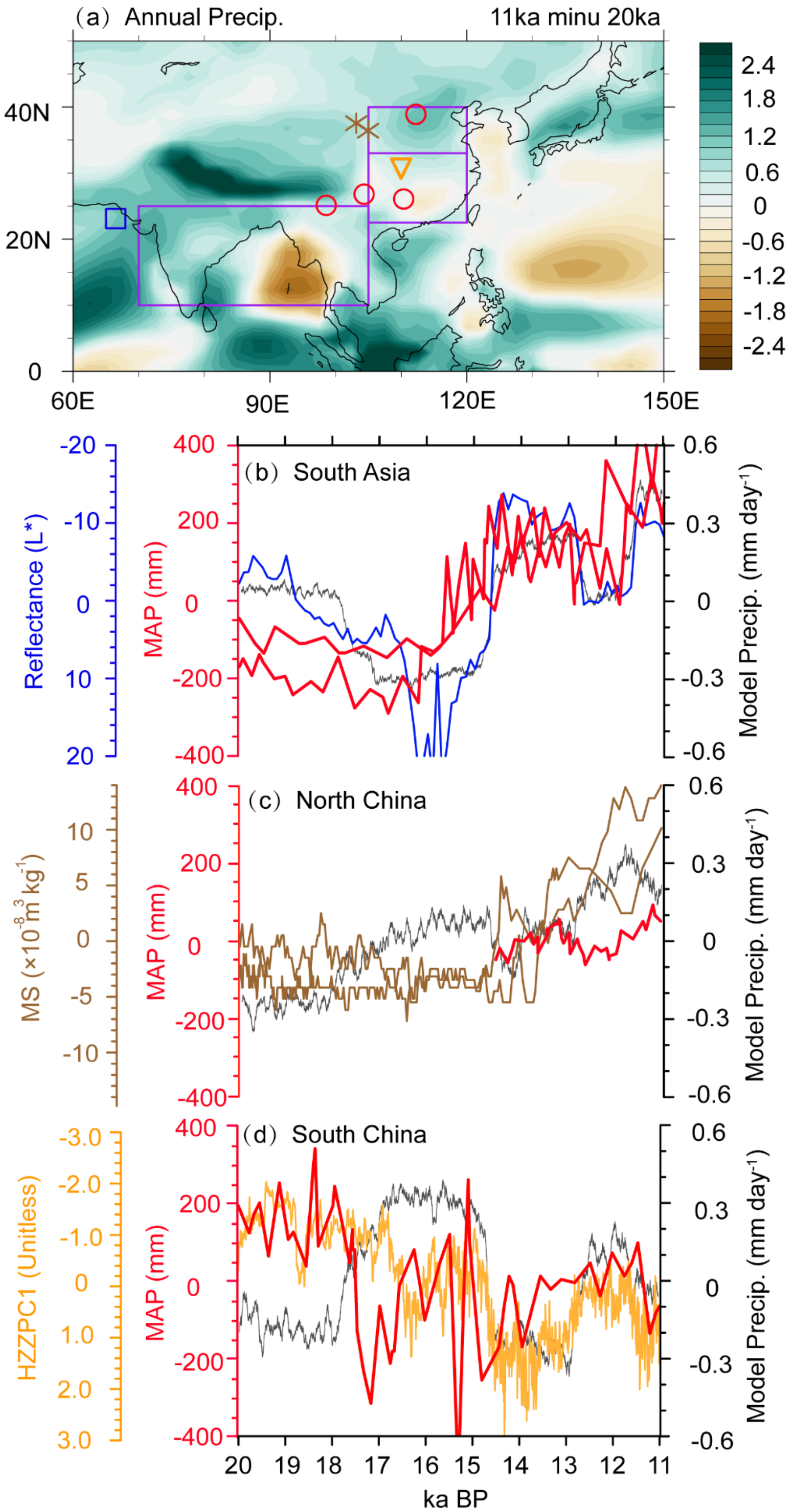

Supplementary Fig. 2 | Pattern and time series of precipitation during the last deglaciation. (**a**) Simulated precipitation difference between the early Holocene and the LGM. Proxy records are marked as follows: pollen (red circles), sediment total reflectance (blue square), loess magnetic susceptibility (brown stars), and speleothem trace elements (yellow triangle). The purple box outlines the South Asia (10–25°N, 70–105°E), north China (22.5–33°N, 105–120°E) and south China (33–40°N, 105–120°E). Shaded areas denote differences that are robust against internal variability ($p < 0.05$, two-tailed Student's *t*-test). Anomaly time series for (**b**) South Asia, (**c**) North China, and (**d**) South China, relative to the long-term mean during the last deglaciation. Proxy records are shown as follows: (**b**) sediment total reflectance at northeastern Arabian Sea[9] (bule) and pollen-based mean annual precipitation from Tengchong Qinghai Lake and Caohai Lake[10] (red); (**c**) loess magnetic susceptibility from Gulang and Jingyuan sections[11] (brown), and pollen-based annual precipitation from Gonghai Lake[12] (red); (**d**) the leading principal component (PC) of Haozhou Cave Mg/Ca, Sr/Ca, and Ba/Ca records[8] (yellow), and pollen-based annual precipitation from Gutian[13] (red). Simulated precipitation (grey) shows the area-averaged precipitation anomaly over land within each corresponding box in (**a**).

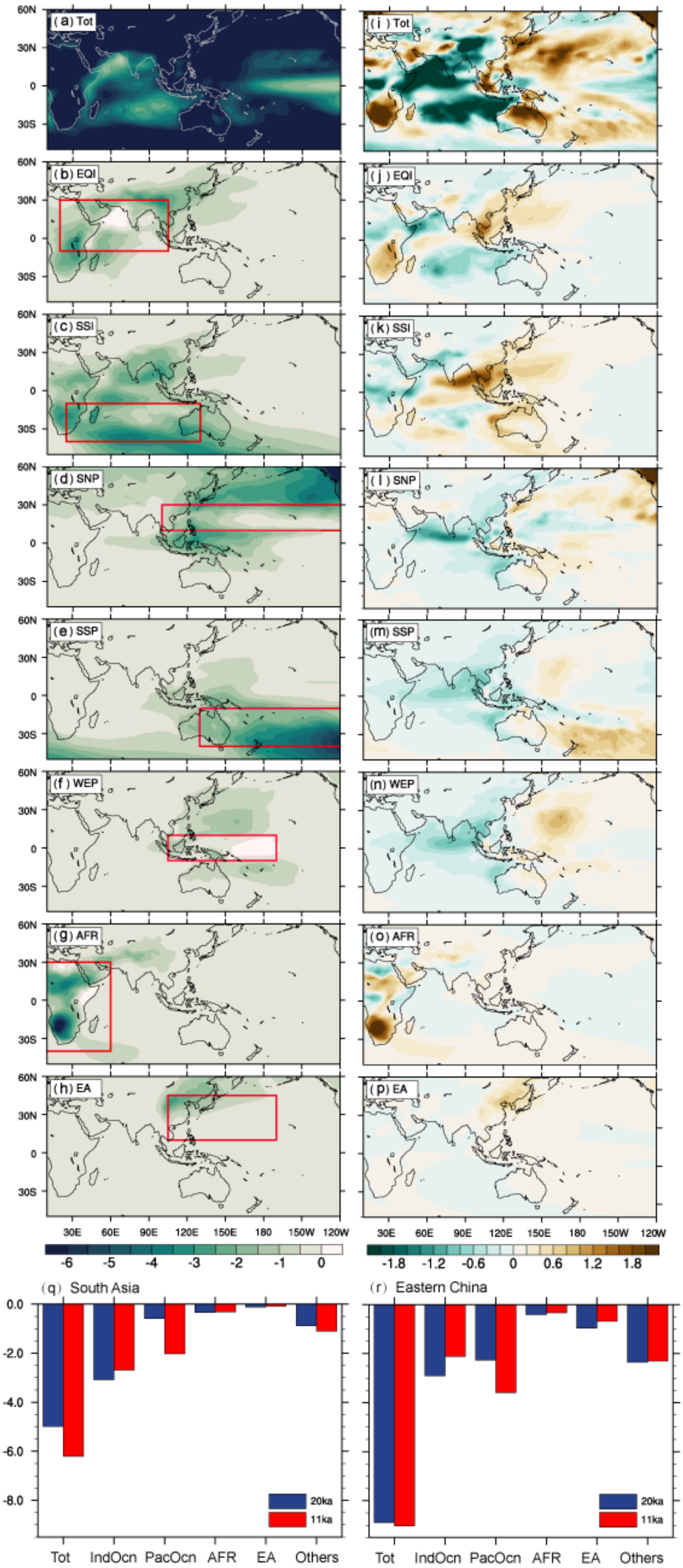

Supplementary Fig. 3 | Climatological and changes of annual $\delta^{18}O_p$ in tagging experiments. (**a–h**) Climatological annual $\delta^{18}O_p$ (‰) at the LGM, originating from the following source regions: global, equatorial Indian Ocean (EQI, 10°S–30°N, 25°–105°E), subtropical South Indian Ocean (SSI, 40°S–10°N, 25°–130°E), subtropical North Pacific Ocean (SNP, 10°–30°N, 105°E–170°W), subtropical South Pacific Ocean (SSP, 10°–40°S, 130°E–110°W), west equatorial Pacific Ocean (WEP, 10°S–10°N, 105°E–170°W), African continent (AFR, 60°S–35°N, 30°W–60°E), and East Asian continent (EA, 10°N–45°N, 105°E–190°E). The source regions are marked by red boxes. (**i**–**p**) Same as (**a**–**h**) but showing the difference between 11 and 20 ka. (**q**) and (**r**) quantify contributions of different source regions to annual $\delta^{18}O_p$ in South Asia and eastern China, respectively. Blue bars represent 20 ka, and red bars represent 11 ka.

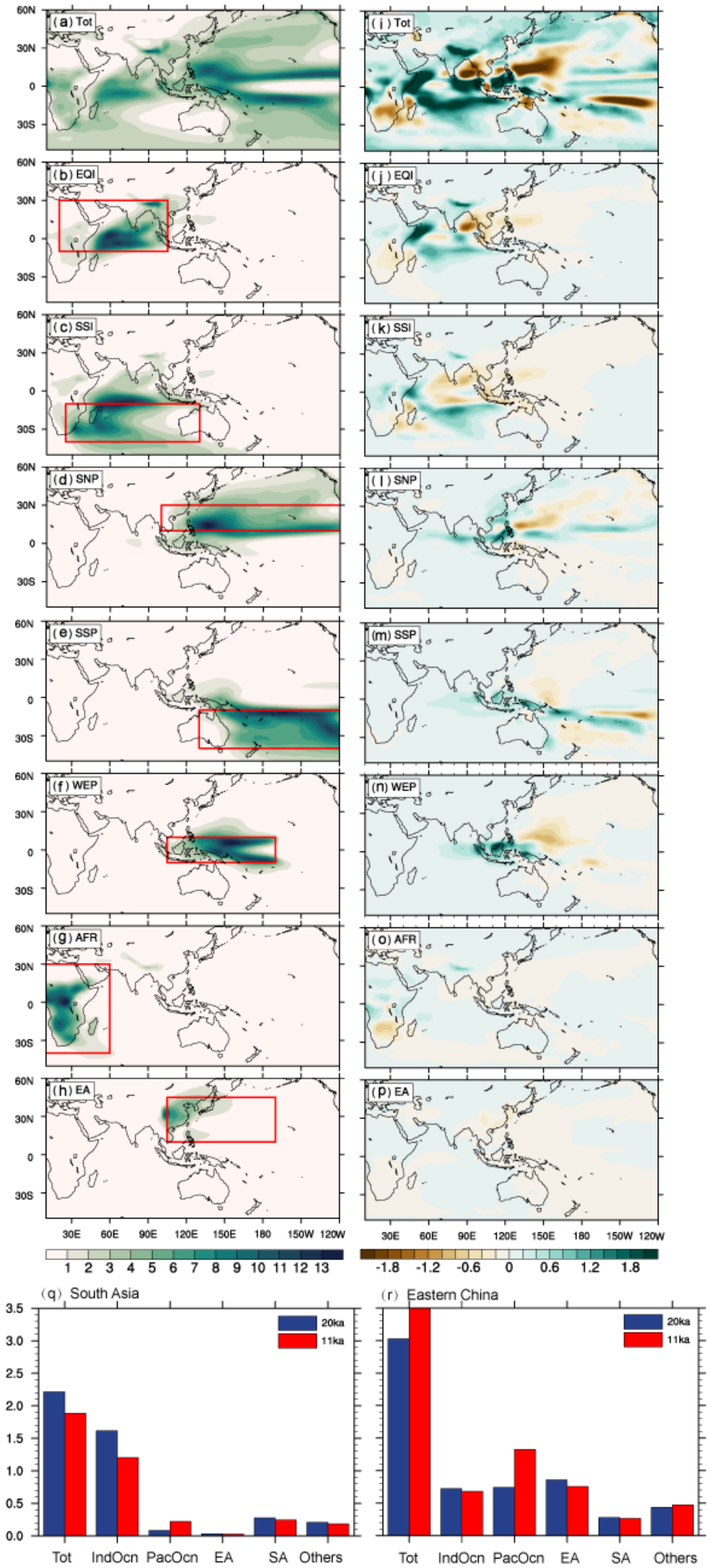

Supplementary Fig. 4 | Climatological and changes of annual moisture (O^{16}) in tagging experiments. Similar to Supplementary Fig. 3, but for precipitation water O^{16} (mm day^{-1}).

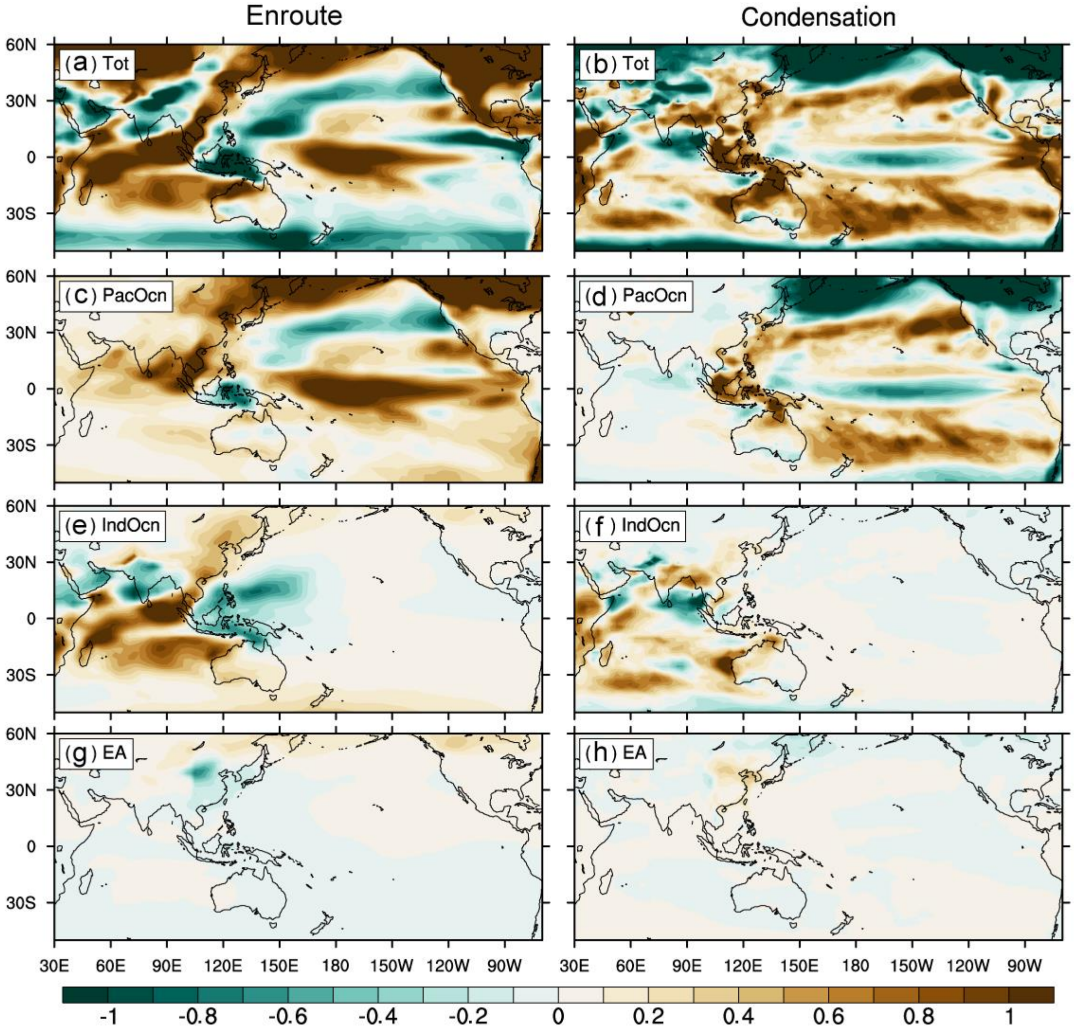

Supplementary Fig. 5 | Decomposition of annual $\delta^{18}O_p$ response between the early Holocene and the LGM. Decomposition of the $\Delta\delta^{18}O_{p,i} \times \frac{P_i}{P}$ term (see Equation 4) into contributions from (**a**) enroute depletion, (**b**) condensation, and source $\delta^{18}O_v$. (**c**), (**e**), and (**g**) denote the impacts of Pacific Ocean, Indian Ocean, and East Asian continent on the enroute depletion term (**a**). (**d**), (**f**), and (**h**) show the impacts of the same source regions on the condensation term (**b**).

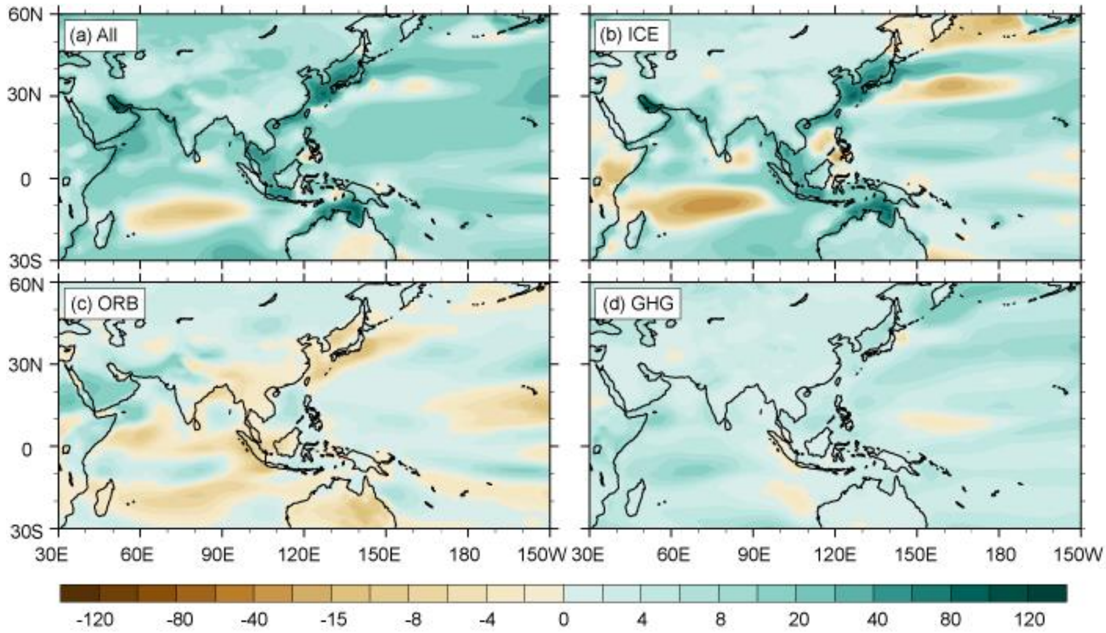

Supplementary Fig. 6 | Changes in latent heat flux between the early Holocene and the LGM under different forcings. The latent heat flux difference (W m^{-2}) for (**a**) All, (**b**) ICE, (**c**) ORB, and (**d**) GHG forcings. Positive (negative) values indicate upward (downward) direction. Shaded areas denote differences that are robust against internal variability ($p < 0.05$, two-tailed Student's *t*-test).

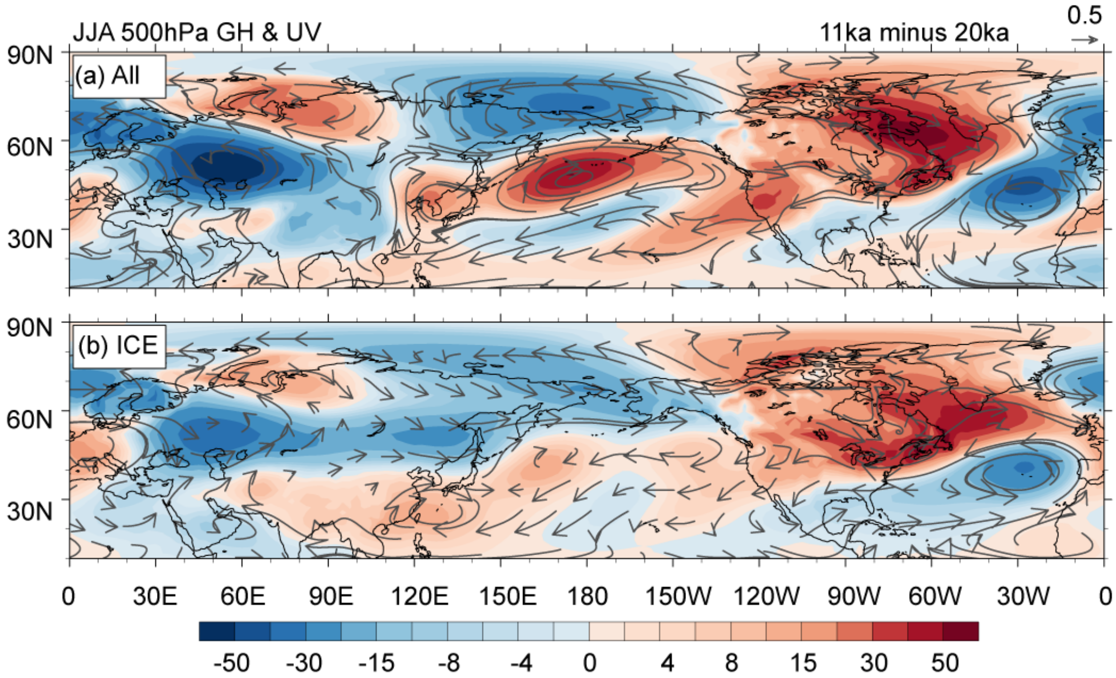

Supplementary Fig. 7 | Upper-level circulation changes between the early Holocene and the LGM. Summer mean 500-hPa eddy geopotential height differences (shading, gpm, represented by the deviation of geopotential height from its zonal mean) and 500h-Pa wind anomalies (vectors, m s^{-1}) in response to (**a**) All and (**b**) ICE forcings. Shaded areas denote differences that are robust against internal variability ($p < 0.05$, two-tailed Student's *t*-test).

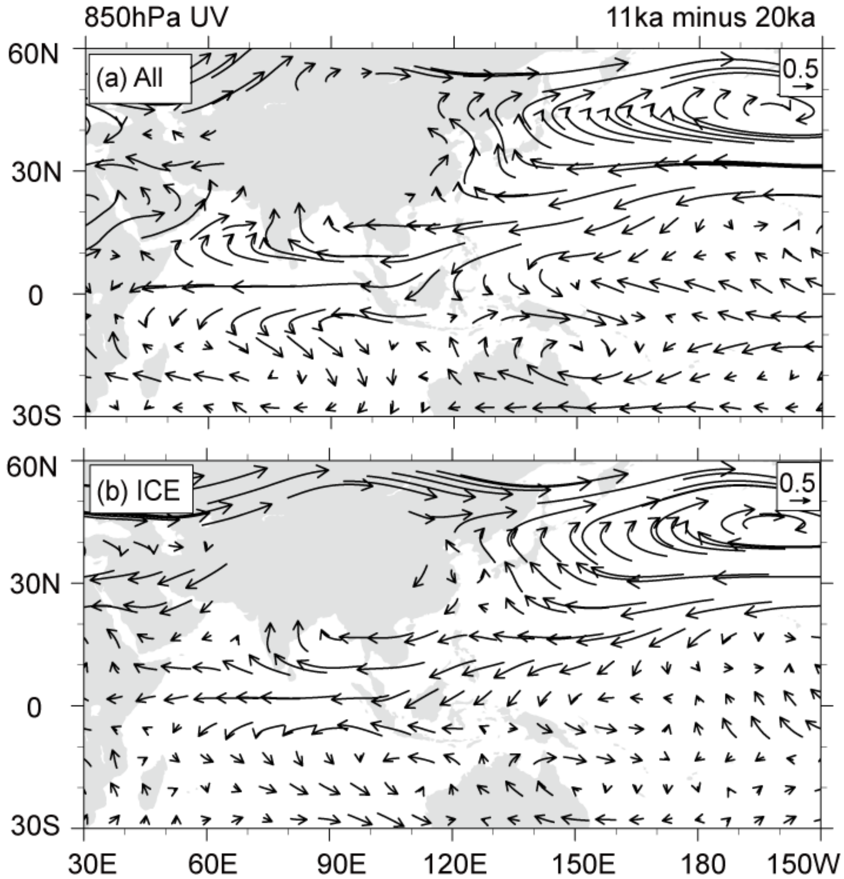

Supplementary Fig. 8 | Patterns of 850-hPa wind changes between the early Holocene and the LGM from TRACE-21ka simulations. (**a**) Response in the all-forcing experiment. (**b**) Response in the ICE forcing experiment.

Supplementary References

1. Liu, G. *et al.* On the glacial-interglacial variability of the Asian monsoon in speleothem δ^{18}O records. *Sci. Adv.* **6**, eaay8189 (2020).
2. Dutt, S. *et al.* Abrupt changes in Indian summer monsoon strength during 33,800 to 5500 years B.P. *Geophys. Res. Lett.* **42**, 5526–5532 (2015).
3. Cai, Y. *et al.* Variability of stalagmite-inferred Indian monsoon precipitation over the past 252,000 y. *Proc. Natl. Acad. Sci. U. S. A.* **112**, 2954–2959 (2015).
4. Li, T.-Y. *et al.* High precise dating on the variation of the Asian summer monsoon since 37 ka BP. *Sci. Rep.* **11**, 9375 (2021).
5. Wang, Z. *et al.* A high-resolution stalagmite record from Luoshui Cave, Central China over the past 23.5 kyr. *Quat. Sci. Rev.* **282**, 107443 (2022).
6. Wang, Y. J. *et al.* A high-resolution absolute-dated late pleistocene monsoon record from Hulu cave, China. *Science* **294**, 2345–2348 (2001).
7. Wu, J., Wang, Y., Cheng, H. & Edwards, L. R. An exceptionally strengthened East Asian summer monsoon event between 19.9 and 17.1 ka BP recorded in a Hulu stalagmite. *Sci. China Ser. D-Earth Sci.* **52**, 360–368 (2009).
8. Zhang, H. *et al.* East Asian hydroclimate modulated by the position of the westerlies during termination I. *Science* **362**, 580–583 (2018).
9. Deplazes, G. et al. Links between tropical rainfall and north Atlantic climate during the last glacial period. *Nat. Geosci.* 6, 213–217 (2013).
10. Zhang, X. et al. Quantification of Asian monsoon variability from 68 ka BP through pollen-based climate reconstruction. *Sci. Bull.* 68, 713–722 (2023).
11. Sun, Y. *et al.* Influence of Atlantic meridional overturning circulation on the east Asian winter monsoon. *Nat. Geosci.* **5**, 46–49 (2012).
12. Chen, F. *et al.* East Asian summer monsoon precipitation variability since the last deglaciation. *Sci. Rep.* **5**, 11186 (2015).
13. Zheng, Z. *et al.* Holocene warming and evergreen/deciduous forest replacement across eastern China. *Quat. Sci. Rev.* **307**, 108057 (2023).